CHALMERS

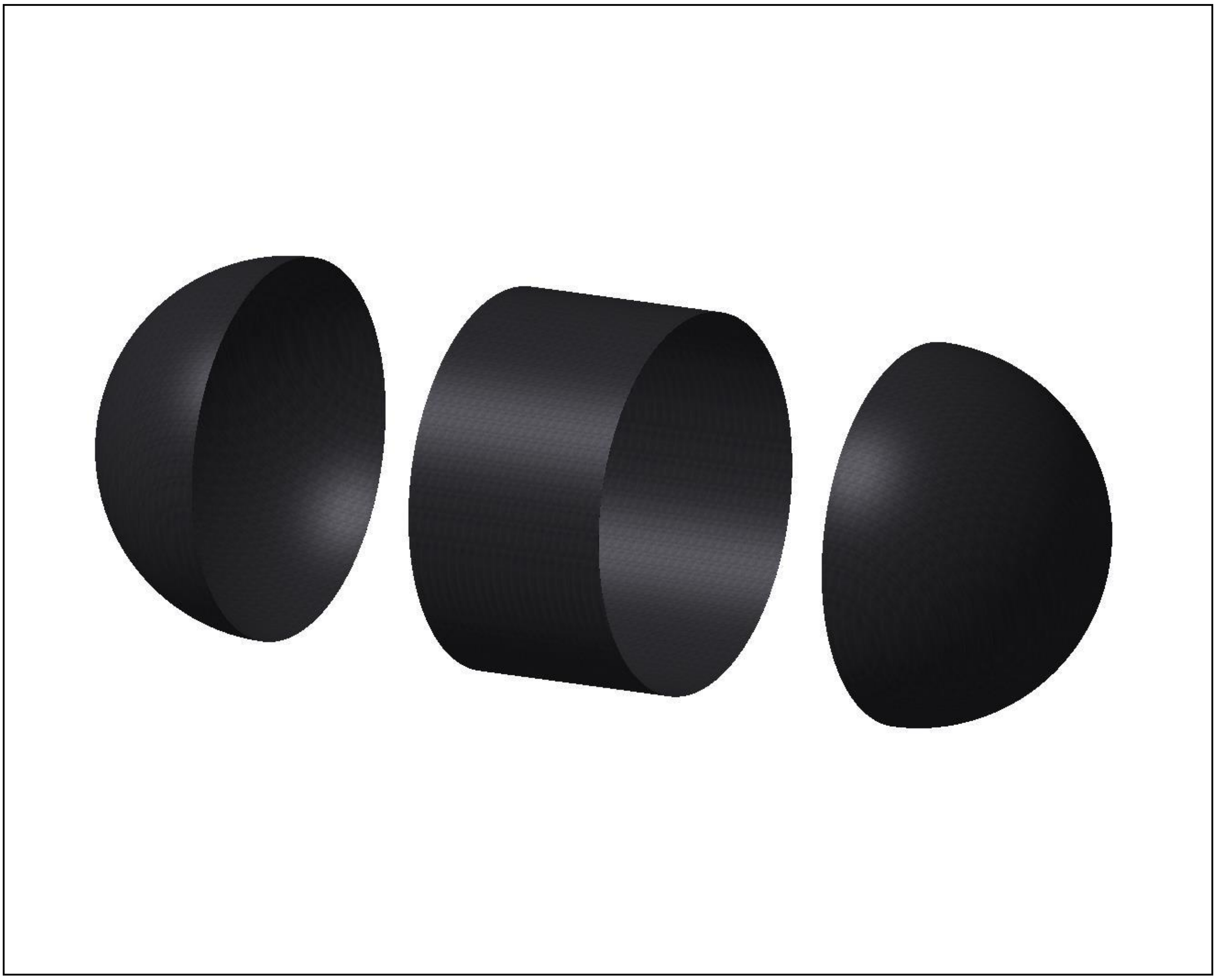

Studentarbeten – Mekanik och maritima vetenskaper (M2) – Projektarbeten
2021:07

Liquid Hydrogen Tanks for Low-Emission Aircraft

TME131 Project in Applied Mechanics 2021

Department of Mechanics and Maritime Sciences
CHALMERS UNIVERSITY OF TECHNOLOGY
Göteborg, Sweden 2021

Liquid Hydrogen Tanks for Low-Emission Aircraft
TME131 Project in Applied Mechanics 2021

Studentarbeten – Mekanik och maritima vetenskaper (M2) – Projektarbeten 2021:07

Department of Mechanics and Maritime Sciences
Chalmers University of Technology
SE-412 96 Göteborg
Sweden
Telephone +46 (0)31 772 1000

Preface

The work in the present report was carried out as a part of the course TME131 Project in Applied Mechanics, which is a mandatory course within the Applied Mechanics Masters programme at Chalmers. The course was carried out during spring semester 2021.

The project was supervised by Prof. Leif Asp (Chalmers University of Technology).

Abstract

Hydrogen power shows high potential in reducing emissions of greenhouse gases from aircraft, which has led to companies investing more of their resources into developing this technology. One of the main issues of this technique is the storing of the liquid hydrogen within the airplane without adding too much weight. This has lead to a demand for designing tanks in carbon fibre reinforced plastics (CFRP). This project has therefore been structured as a pre-study to further increase the knowledge available on the design of liner-less composite pressure vessels.

It was discovered that a liner-less pressure vessel made out of thin-ply composite material is a concept of great potential. The two sections of the proposed tank, the tube, and the two endcaps were constructed differently. In terms of stress and strain, they both indicated potential complying to limits set on the material, both in terms of ultimate values and thermal fatigue. Connecting the two main parts through a single scarf joint, currently common within the aerospace industry, the overall weight of the tank was decreased with a factor of over 85% compared to a steel tank. In conclusion, the design of a liner-less composite tank shows great potential and it is of interest to conduct further research in this area.

Table of Contents

1 Introduction

This chapter provides an introductory overview of the project including the aim, limitations, background, and a review of state-of-the-art technologies currently discussed within the industry.

1.1 Background

During July of 2020, the European Union launched a strategy for carbon-free production of hydrogen on a large scale where hydrogen acts as a main pillar in meeting the climate goals of 2050 [1]. This in turn led to the commercial aircraft manufacturer Airbus setting a target for 2035 to have an aircraft running on liquid hydrogen (LH2) ready for service [2]. The main advantage of using liquid hydrogen as fuel is that there are no greenhouse gases being emitted, the product is water vapour and a small amount of NO_x [3]. If the hydrogen is produced using renewable energy sources, the usage of it as a fuel will have a minimal impact on global warming. The main drawback, however, with liquid hydrogen is that it has approximately four times lower volumetric energy density compared to standard jet fuel, meaning the LH2 tanks have to be four times larger by volume than the conventional kerosene tanks to have the same range [4]. This makes the storing of liquid hydrogen more problematic for designing new aircraft.

Liquid hydrogen is around -253 °C when stored. This is a big difference compared to the minimum temperature of standard jet fuel which has a freezing temperature of -40 °C to -50 °C depending on the type of fuel [5]. Considering how high the temperature is outside of the storage tank (outdoor temperature) high demands are put on the material properties of the tank. Not only does the material need to be able to withstand the low temperature without breaking but it also has to be able to handle potential thermal fatigue caused by the refuelling process. When the tank is empty the temperature will be considerably higher compared to when the tank is full. If the tank is assumed to have the same temperature as the ambient air when it is empty the temperature difference could be well over 300 °C.

For many years, cryogenic metal tanks have been used to store cold substances. By using thin-ply (<60 μm) composite tanks it has been indicated by NASA (National Aeronautics and Space Administration) and the CHATT (Cryogenic Hypersonic Advanced Tank Technologies)-project that the weight of the tank can be reduced by as much as 30% [6]. This is a significant decrease that would contribute towards potentially reducing fuel consumption. The reason for this is mainly due to the fact that carbon fibre reinforced plastic (CFRP) generally is much stronger in the fibre direction compared to metals [7]. If the orientation of these fibres is optimised in relation to the load case, the product will be very lightweight and strong. For liquid hydrogen storage tanks, the boundary conditions are well known and defined allowing for a high level of optimisation. In addition, the potential for cracks and resulting leakages can be minimised when using thin-ply composites [8]. Usually, a carbon-fibre liquid hydrogen tank will have an inner liner to prevent permeation. By eradicating the need for an inner liner the weight of the tank can be reduced significantly by making the tank liner-less.

The project will focus on making a preliminary design for a liquid hydrogen tank made out of thin-ply composite material. There is a company in Borås, Sweden, called Oxeon AB that specialises in manufacturing thin-ply composites. They can achieve a ply-thickness of only 20 μm with their brand TeXtreme©. This project was performed in collaboration with Airbus and Oxeon.

1.2 State of the Art

There is an interest in the development of liquid hydrogen tanks within the aeronautical and space industry. This leading to multiple studies being conducted on the topic with the objective to further increase knowledge within the area. This section briefly covers current knowledge and concepts available on the topic that was found relevant to the progress of the project and its objective.

The current state-of-the-art pressure vessels used around the world are mainly based on metal tanks for containing liquids and gases. Usage of metal tanks are widespread and common due to their simplicity in production and consistent structural integrity. However, the metal vessels are heavy and do not use the material effectively due to them being designed to comply with the largest stress (in the hoop direction of the cylinder). In the last decades, the capability to manufacture thin-ply composites has increased with recent studies indicating the possibility to use this as a substitute for steel [9]. Studies have shown that through implementation of composite materials in the design it is possible to develop pressure vessels that have improved pressure capacity, reduced weight and produce highly performing tanks in terms of structural integrity [10]. There is therefore a general interest among aircraft manufacturers to further explore thin-ply composites for realisation of lightweight LH2 tanks.

The multinational collaboration through the CHATT project was one major research collaboration with the aim to investigate CFRP cryogenic pressure tanks. Within the study, it is mentioned that the reduction of weight and improved structural performance is the main aim of this implementation. The study assesses the different advantages and disadvantages of using liner/liner-less tank designs with standard as well as more complex geometries [11]. Currently, it is common to use a metal liner or internal structure with the use of a composite overwind [12]. In the CHATT project there also examples where the endcaps are made out of metal and then adhesively bonded onto a CFRP-liner.

1.3 Aim

The aim of the project is to propose and analyse a preliminary design for a lightweight liquid hydrogen tank. This is accomplished through the proposal of a tank design and feasible manufacturing methods when using thin CFRP as the source material. Providing calculations on the strength of the tank and give an insight into its separate components is the core of the project.

The aim is further detailed by proposing a tank without the use of a metal liner. Due to a noticeable lack of available studies on this, it is of interest to provide further knowledge in this area. The tank must be able to withstand a pressure of 4 bar and an internal temperature difference from 130 °C (common curing temperature of CFRP) to -253 °C (boiling temperature of hydrogen).

1.4 Project Boundaries

In order to ensure that the set objective is reached, multiple limitations were implemented to frame the scope. In this section, the limitations for the 10-week project are detailed.

1.4.1 Material Choice

For this project, the chosen model material is the T800S carbon fibres made by Toray in combination with the #2592 epoxy matrix. T800S is an intermediate modulus carbon fibre that is believed to have suitable properties for the intended application. Material data for the combination of the T800S fibres and the #2592 epoxy matrix are readily available. Important to note is that the laminate will be made of thin-plies (down to 20 μm) since the thickness of the plies has a big impact on the material properties and failure modes of the final product. In terms of matrix and fibre data, they are found in Table 1. The variables are denoted as $\bullet_*$ where the subscript $*$ represents f for fibre data and m for matrix data. The data is mainly provided by the T800S datasheet from Toray. Data required which was not found in the datasheet, e.g. the matrix Poisson's ratio ν_m and coefficient of thermal expansion (CTE) α_m, was instead filled in by reasonable assumptions provided by supervisor Leif Asp.

Table 1: Material data, #2592 epoxy matrix - T800S carbon fibres.

	Tensile modulus E_* [GPa]	CTE α_* [10^{-6}/°C]	Volume fraction V_*	Poisson's ratio ν_*	Density ρ_*[kg/m^3]
Matrix	3.2	62	0.4	0.35	1110
Fibre	294	-0.4	0.6	0.24	1800

1.4.2 Design Limitations

The designs and results produced in this project will be purely digital in the shape of CAD models, FE-modelling and hand calculations. No prototypes or other physical models will be made. The components studied within this project are the tube, endcaps, and the joint between them. The tank will also be assumed to be insulated and outer elements such as turbulence, landing impact, wind drag, and structural fittings will not be taken into consideration. In addition, hygroscopic (moisture) effects on the material are out of scope.

Considering the magnitude of work related to the design of a liquid hydrogen tank the geometrical properties of the tank will be predetermined. This allows for more resources to be used for the lay-up design. The volume of the proposed tank has been chosen based on the aircraft Boeing 737 Max-10 which has a fuel capacity of 25 817 litres. The max distance for the 737 Max-10 is 3300 nautical miles (NM) which would theoretically last 7 round flights between Gothenburg and Stockholm (430 NM each) with fuel to spare [13]. Considering that the liquid hydrogen requires four times the volume the predetermined value is set to last for fewer flights [4]. For the sake of simplicity, the liquid hydrogen tank was therefore set to be the same volume as the regular fuel capacity of the Boeing 737 Max-10.

1.5 Report Outline

Following this introductory chapter which describes the background and defines the scope of the project comes the main part of the report. The main part includes chapter 2, *Tank Design* and chapter 3, *Proposed Routes for Manufacturing.* The tank design chapter initially sets the global design of the tank and is followed by in depth analyses of the tube, endcaps and joint including method, theory, results and discussion of each individual part. The tank design chapter ends with a weight analysis and comparison to a steel tank and is followed by an analysis of the possible routes for manufacturing. Finally conclusions are drawn and suggestions for future work are stated as the end of the report.

2 Tank Design

There are a lot of uncertainties in the future of hydrogen fuelled aircraft. There are multiple prototype designs of hydrogen fuelled airplanes with different designs and different tank placements. Some prototypes are very futuristic and some are simply re-designs of commercial aircraft where the tanks have been changed and moved [2]. The design of the tank depends on the airplane and the placement of the tank. In some cases, a long and slender tank with spherical endcaps might be the best choice, other airplanes might require a shorter tank with elliptical endcaps. If the tank is placed in the back of the fuselage, a conical shape could be advantageous.

The most common type of tank is a cylindrical one but the length of the cylinder and the shape of the endcaps may vary. Some different types of endcaps are: hemispherical, semi elliptical and flat, shown as assemblies in Figure 1. Of these three endcap shapes, the hemispherical one provides the best internal volume to surface area ratio and it also requires the lowest wall thickness [14]. On the other hand, it also wastes the largest amount of external volume if one imagines it to fit in a box. Therefore, the design of the tank and the airplane must be compatible to use the space as efficiently as possible.

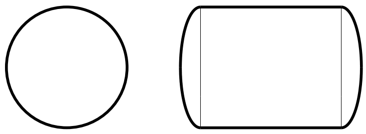

(a) Cylindrical tube with semi-elliptical endcaps.

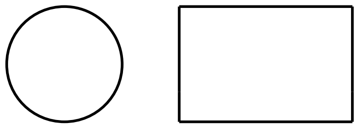

(b) Cylindrical tube with flat endcaps.

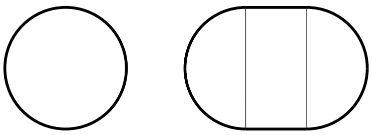

(c) Cylindrical tube with hemispherical endcaps.

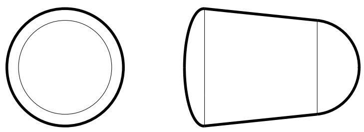

(d) Conical tube with semi-elliptical and hemispherical endcaps.

Figure 1: Tank designs, combinations of tube and endcap shapes, side and front view.

Considering that one of the main goals is to design a lightweight tank, the hemispherical endcaps were chosen to be used for this design. The final design of the tank is shown in Figure 2. It is a cylindrical tube with hemispherical endcaps and has the cylinder length $L_c = 1.7$ m and the diameter $D = 3$ m which gives the internal volume $V = 25.2$ m^3.

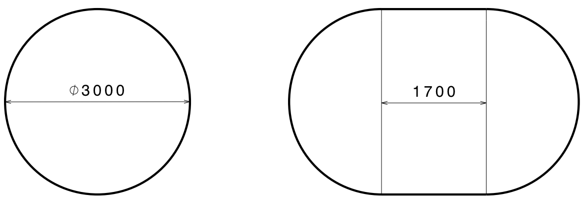

Figure 2: Final tank design, cylindrical tube with hemispherical endcaps.

2.1 Tube

In this section, the tube part of the tank was analysed both analytically using MATLAB and numerically using the commercial FE-software Abaqus. The first step was to determine a layup for the CFRP material that could withstand the applied pressure, 4 bar, and temperature change, $\Delta T = -383$ °C, as mentioned in Section 1.3. This was done by optimisation in MATLAB for different layups. The curing temperature, 130 °C is the stress-free state in the composite with respect to temperature. The resulting local stresses in the chosen composite layup were determined in both MATLAB and Abaqus. In addition, a fatigue analysis was done for a decreased temperature change, $\Delta T = -253$ °C, ranging from 0 °C to -253 °C. Since it is unknown whether or not liquid hydrogen tanks for aircraft will be emptied on a regular basis this temperature difference was set as an example, where the maximum allowed temperature can be outlined in the operational guidelines of the tank. Here the strains were of more interest with a fatigue strain limit being set to $\epsilon_m = 0.6$ % taken from an article by Talreja [15], where below the fatigue strain limit, no fatigue occurs.

2.1.1 Method and Theory - Tube

In a conventional thick ply composite, the transverse strength is much lower than the longitudinal strength. In general when the ply thickness is reduced to below 60 μm (thin-ply limit), the transverse and shear strength increases and ultimately fibre failure is critical [8]. Since the tube will be made out of thin-ply composites the shear and transverse strength was estimated to be 4.8 times stronger than thick-ply unidirectional composites [16]. The new values can be seen in Table 2 together with material data for T800S - #2592 epoxy composite provided by the manufacturer Toray. Subscripts L and T denote longitudinal and transverse ply directions respectively and U denotes ultimate strength.

Table 2: Lamina properties, thin-ply, 2592 epoxy matrix - T800S carbon fibres.

E_L [GPa]	E_T [GPa]	σ_{LU} [MPa]	σ_{TU} [MPa]	τ_{LTU} [MPa]
163	17	3290	379	648

In order to make analytical calculations for the tube classical laminate theory (CLT) was used. This allowed for determination of mechanical properties of individual composite plies placed on top of each other to form a composite laminate. In order to apply CLT the tube was thought of as a cylinder constructed by connecting two of the ends of a laminate and hence creating a cylindrical shape.

In Equations (1) to (16) from CLT, Table 1 was used for the fibre and matrix data for the elastic modulus, Poisson's ratio, volume fraction and thermal expansion coefficient. All the equations were taken from the book "Analysis and Performance of Fiber Composites" [7]. The transverse and shear moduli in local coordinates of a lamina were determined using the Halpin-Tsai model:

$$E_T = E_m \frac{1 + \xi\eta V_f}{1 - \eta V_f}, \quad \eta = \frac{(E_f/E_m) - 1}{(E_f/E_m) + \xi}, \quad \xi = 2 \tag{1}$$

$$G_{LT} = G_m \frac{1 + \xi\eta V_f}{1 - \eta V_f}, \quad \eta = \frac{(G_f/G_m) - 1}{(G_f/G_m) + \xi}, \quad \xi = 1 \tag{2}$$

The shear moduli used were found by assuming isotropic behaviour of the constituents.

$$G_f = \frac{E_f}{2(1+\nu_f)}, \quad G_m = \frac{E_m}{2(1+\nu_m)} \tag{3}$$

The rule of mixtures model was used next to compute the minor and major Poisson's ratios in local coordinates and the density of the composite material.

$$\nu_{LT} = \nu_f V_f + \nu_m V_m, \quad \nu_{TL} = \nu_{LT}\frac{E_T}{E_L} \tag{4}$$

$$\rho_c = \rho_f V_f + \rho_m V_m \tag{5}$$

The longitudinal stiffness of a lamina can also be calculated using the rule of mixtures model but it was given for the chosen material.

In order to account for thermal effects on the material the thermal expansion coefficients were determined as

$$\alpha_L = \frac{1}{E_L}(\alpha_f E_f V_f + \alpha_m E_m V_m) \tag{6}$$

$$\alpha_T = (1+\nu_f)\alpha_f V_f + (1+\nu_m)\alpha_m V_m - \alpha_L \nu_{LT} \tag{7}$$

In composite mechanics the lamina stiffness is represented by a 3x3-matrix in the following way:

$$[\mathbf{Q}] = \begin{bmatrix} \frac{E_L}{1-\nu_{LT}\nu_{TL}} & \frac{\nu_{LT}E_L}{1-\nu_{LT}\nu_{LT}} & 0 \\ \frac{\nu_{LT}E_T}{1-\nu_{LT}\nu_{LT}} & \frac{E_T}{1-\nu_{LT}\nu_{LT}} & 0 \\ 0 & 0 & G_{LT} \end{bmatrix} \tag{8}$$

The stiffness matrix $\mathbf{Q}$ is defined in local (L, T) coordinates. In order to express it in global coordinates transformation matrices needed to be used, where Φ is the ply angle:

$$[\mathbf{T_1}] = \begin{bmatrix} \cos^2\Phi & \sin^2\Phi & 2\sin\Phi\cos\Phi \\ \sin^2\Phi & \cos^2\Phi & -2\sin\Phi\cos\Phi \\ -\sin\Phi\cos\Phi & \sin\Phi\cos\Phi & \sin^2\Phi - \cos^2\Phi \end{bmatrix} \tag{9}$$

$$[\mathbf{T_2}] = \begin{bmatrix} \cos^2\Phi & \sin^2\Phi & \sin\Phi\cos\Phi \\ \sin^2\Phi & \cos^2\Phi & -\sin\Phi\cos\Phi \\ -2\sin\Phi\cos\Phi & 2\sin\Phi\cos\Phi & \cos^2\Phi - \sin^2\Phi \end{bmatrix} \tag{10}$$

The forces applied to the material were implemented by analysing the whole laminate using Equation (11) where the ABD-matrix acts as a laminate stiffness matrix.

$$\begin{Bmatrix} \mathbf{N} \\ \mathbf{M} \end{Bmatrix} = \begin{bmatrix} \mathbf{A} & \mathbf{B} \\ \mathbf{B} & \mathbf{D} \end{bmatrix} \begin{Bmatrix} \epsilon^0 \\ \mathbf{k} \end{Bmatrix} \tag{11}$$

Here ϵ^0 is the mid-plane strains of the laminate and $\mathbf{k}$ is the curvature of the laminate. The expressions for the $\mathbf{A}$, $\mathbf{B}$ and $\mathbf{D}$ matrices individually are shown below. As can be seen the matrices are constructed of n number of individual lamina where the thickness of a trivial lamina is expressed as $h_k - h_{k-1}$.

$$\mathbf{A} = \sum_{k=1}^{n} [\bar{\mathbf{Q}}]_k (h_k - h_{k-1}) \tag{12}$$

$$\mathbf{B} = \frac{1}{2}\sum_{k=1}^{n}[\bar{\mathbf{Q}}]_k(h_k^2 - h_{k-1}^2) \tag{13}$$

$$\mathbf{D} = \frac{1}{3}\sum_{k=1}^{n}[\bar{\mathbf{Q}}]_k(h_k^3 - h_{k-1}^3) \tag{14}$$

For the **A**, **B** and **D** matrices $\bar{\mathbf{Q}} = \mathbf{T}_1^{-1}\mathbf{Q}\mathbf{T}_2$ is the lamina stiffness in global coordinates.

The final step was to use the calculated material properties and the stiffness matrices to determine the strains and stresses both locally and globally for the laminate. Without taking any hygroscopic effects into consideration the strains and stresses for each individual ply can be computed by the two equations below, where z is the z-coordinate through the laminate thickness.

$$\begin{Bmatrix} \epsilon_x^M \\ \epsilon_y^M \\ \epsilon_{xy}^M \end{Bmatrix}_k = \begin{Bmatrix} \epsilon_x^0 + zk_x \\ \epsilon_y^0 + zk_y \\ \epsilon_{xy}^0 + zk_{xy} \end{Bmatrix} - \begin{Bmatrix} \alpha_x \\ \alpha_y \\ \alpha_{xy} \end{Bmatrix}_k \Delta T \tag{15}$$

$$\begin{Bmatrix} \sigma_x \\ \sigma_y \\ \sigma_{xy} \end{Bmatrix}_k = [\bar{\mathbf{Q}}]_k \begin{Bmatrix} \epsilon_x^0 + zk_x \\ \epsilon_y^0 + zk_y \\ \epsilon_{xy}^0 + zk_{xy} \end{Bmatrix} - [\bar{\mathbf{Q}}]_k \begin{Bmatrix} \alpha_x \\ \alpha_y \\ \alpha_{xy} \end{Bmatrix}_k \Delta T \tag{16}$$

Under the assumption that the tank is thin walled ($t \ll r$), the global stresses can be calculated analytically using the pressure vessel formulas in a cylindrical coordinate system.

$$\sigma_\varphi = \frac{pr}{t}, \quad \sigma_z = \frac{pr}{2t}, \quad \sigma_r = 0 \tag{17}$$

Where t is the wall thickness, p is the internal pressure, r is the radius and denotes the radial direction, z is the axial direction along the tube and φ is the angular direction. In order to find a suitable composite layup for the tube a MATLAB program was written using CLT and the stresses from the pressure vessel formulas. The program tested different ply patterns with two varying angles and repeated theses patterns until a reasonable thickness was achieved. The layups that were tested were:

$$[\alpha/\beta]_{50}, \quad [\alpha/90/\beta]_{34}, \quad [\alpha/0/\beta]_{34}, \quad [\alpha/\beta/\alpha]_{34}, \quad [\alpha/\beta/-\alpha]_{34}$$

The maximum stresses in local coordinates and the strain in the hoop-direction (global coordinates) were saved for all α and β values. The hoop strain is particularly relevant for the joint. Any difference in radial displacement between the tube and the endcaps would put a large strain on the joint.

For the numerical analysis, the first step was to import a cylindrical shell model into Abaqus, using the dimensions stated in Section 2. The imported model was created using CATIA V5, the reasoning behind using a shell model is that the elements are very thin in relation to their surface area. This model type was also recommended by the co-supervisor Robert Auenhammer. An alternative would have been to use smaller elements with a more even length to depth ratio [17]. The number of integration points was set to three. The layup was implemented using an optimal layup from the analytical calculations. Due to symmetry, it is not necessary to model the whole tube but the computational time was insignificant and thereby there was no need to reduce the model.

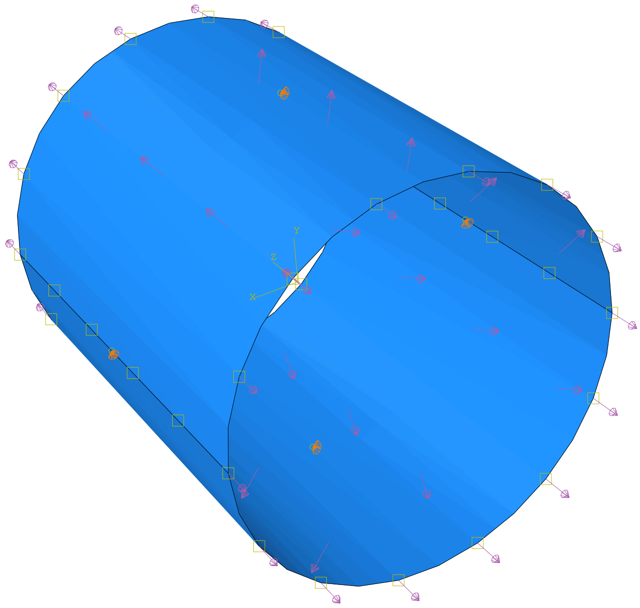

Figure 3: View of Abaqus tube model with applied boundary conditions and forces.
● - surface/edge pressure, ● - fixed displacement, ● - temperature.

The boundary conditions and loads were set according to Figure 3. To stop rigid body motion occurring four nodes were locked in two translations illustrated by the orange supports in Figure 3. The free translation was set in the direction normal to the surface of the cylinder. When inspecting the first results it became apparent that the constrained nodes had to be located exactly at the midpoint along the cylinder length. Otherwise, the stresses and deformations would not be completely symmetric and give slightly skewed results. The applied loads consisted of an internal pressure on the inside area of the tube and a shell edge load applied along both ends of the tube, both represented by purple arrows in Figure 3. The value for the pressure was 4 bar and the shell edge loads were set to 300 N/mm along the circumference, calculated analytically using the pressure vessel formulas (Equation (17)). The temperature change was not added as a load but as a predefined field ranging from 130 °C to -253 °C illustrated by the yellow squares.

Finally, a mesh convergence study was performed to determine how many elements were needed to achieve convergence for the results. The results used were the local stresses in each ply in the longitudinal, transverse and shear direction. The maximum radial and axial displacements were also used.

2.1.2 Results - Tube

In Table 3 analytical results for different layups are presented for 102 plies. The number of plies was set with the tank requirements and with the least common denominator of the two and three angle layups in mind. When comparing the stress result with the material data in Table 2 the stress in the transverse direction was found to be the most critical. For this reason, the layups presented in Table 3 are the result for each pattern providing the lowest value of σ_T. There are some effects that need to be considered when looking at the analytical results, most notably the pattern $[\alpha/90/\beta]_{34}$ which gives the result $[90/90/90]_{34}$ for lowest σ_T. Since there is no angle difference in the plies there will be no thermal stresses and the temperature difference will only result in a free contraction. A layup with no change of ply angle can be seen as one single ply. This would result in the assumption of thin-ply composites no longer being valid.

Table 3: Analytical result from MATLAB for the lowest σ_T.

pattern	layup	plies	σ_L $[MPa]$	σ_T $[MPa]$	τ_{LT} $[MPa]$	ϵ_2 [%]
$[\alpha/\beta]_{51}$	$[68/-68]_{51}$	102	299.5	144.3	± 26.8	0.28
$[\alpha/90/\beta]_{34}$	$[90/90/90]_{34}$	102	294.1	147.1	0	0.15
$[\alpha/0/\beta]_{34}$	$[90/0/90]_{34}$	102	323	236.3	0	0.16
$[\alpha/\beta/\alpha]_{34}$	$[74/-68/74]_{34}$	102	296.9	144.9	± 23	0.24
$[\alpha/\beta/-\alpha]_{34}$	$[-71/-71/71]_{34}$	102	339.4	146.5	± 24.2	0.24

In the layups $[90/0/90]_{34}$, $[74/-68/74]$ and $[-71/-71/71]$ double layers occur. This leads to a reduction in the transverse and shear strength in order for thin-ply assumption to be valid. The best layup with the lowest transverse stress and best transverse strength was a pattern with [68/-68]. In order to remove the stress concentration at the inner and outer boundary of the wall, the layup was changed to be symmetric around the midplane. This results in one double layer in the middle of the laminate but the effect of this should be negligible. To ensure that the mechanical strain is below the fatigue threshold a total of 152 plies was needed, further discussed later in the section. As a result, the final layup is $[(68/-68)_{38}]_s$ with a wall thickness of 3.04 mm which validates the thin-walled assumption in Section 2.1.1.

In Table 4, analytical and numerical results for the tube layup are presented and the values are identical. The table shows the longitudinal stress (σ_L), the transverse stress (σ_T) and the shear stress (τ_{LT}) for each ply as well as the radial displacement (U_r) of the tube. When comparing these values with the strength values shown in Table 2, the stresses are well below the strength limits. Even when multiplying with a safety factor of 2.5, suggested by Peter Linde [18], only the transverse stress ($110 \cdot 2.5 = 275$ MPa) is approaching its strength limit (379 MPa).

Table 4: Analytical and numerical results for the selected $[(68/-68)_{38}]_s$ layup with a change in temperature ΔT = -383 °C and internal pressure 4 bar.

	σ_L [MPa]	σ_T [MPa]	τ_{LT} [MPa]	U_r [mm]
MATLAB	186	110	± 32	3.5
Abaqus	186	110	± 32	3.5

The predicted magnitude of displacement for the tube is plotted in Figure 4, with an exaggerated visual deformation. The grey mesh is showing the undeformed mesh making it obvious that the tube shrinks in the axial direction and expands in the radial direction.

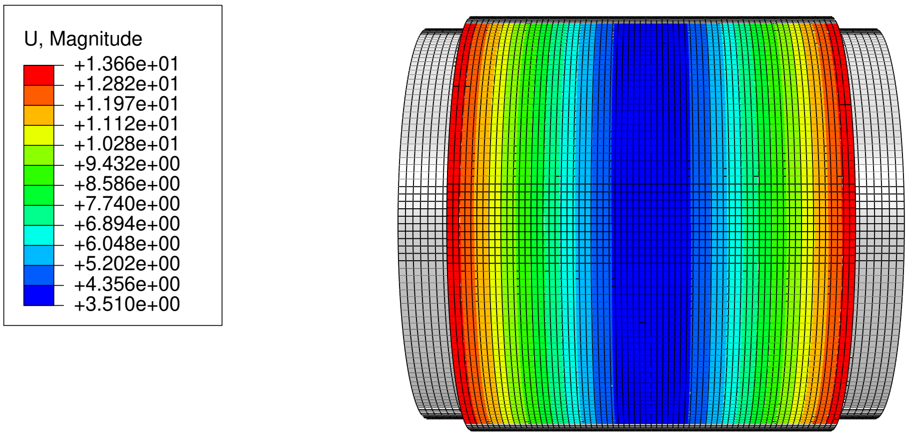

Figure 4: Magnitude of displacements shown in a front-view for the tube in Abaqus.

For the fatigue analysis the strains were approximated linearly using Hooke's law: $\epsilon = \sigma/E$. The elastic moduli for different directions used came from the calculations in MATLAB except for E_L which was given. The local stresses computed in MATLAB and Abaqus were identical, this was also the case for the strains as shown in Table 5. The maximum strain was in the transverse direction, 0.58 %, which is below the fatigue strain limit of 0.6 %.

Table 5: Predicted strains in the tube from MATLAB and Abaqus due to a change in temperature ΔT = -253°C and internal pressure of 4 bar.

	ϵ_L [%]	ϵ_T [%]	ϵ_{LT} [%]
MATLAB	0.12	0.58	±0.38
Abaqus	0.12	0.58	±0.38

Finally, the result from the convergence study is shown in Figure 5. The study was started with a total number of elements of 16, roughly increasing by a factor of four up until reaching 12784 elements. All terms investigated converged fast and most of them were close to their converged value from the start.

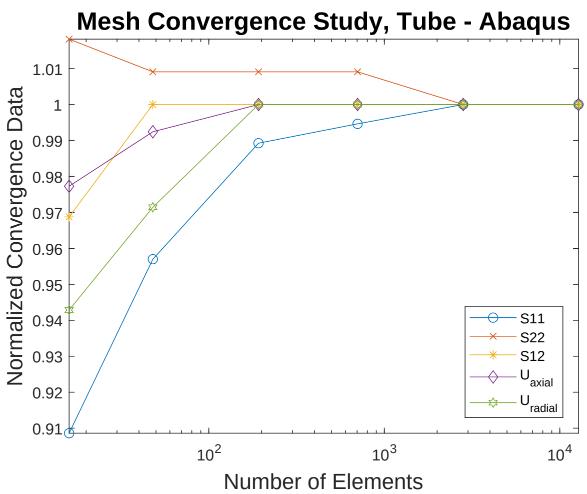

Figure 5: Graph showing convergence with increasing number of elements for normalised units.

2.2 Endcaps

Each endcap of the tank is hemispherical in shape and has a radius of $r = 1.5$ m, shown in Figure 2. The materials used in the endcaps were the same as for the tube, T800S carbon fibres combined with a #2592 epoxy matrix. The layup of the plies however is not at all similar. A uniformly oriented ultra-thin CFRP tape composite, previously investigated experimentally and analytically by Marcus Johansen [19] and Mattias Persson [16] respectively was used for the endcaps. This layup was chosen due to its ease of manufacture, in-plane isotropic properties, and use of thin-plies that prevent transverse cracks to initiate and coalesce, and hence reduce the risk for permeation of the liquid hydrogen. The composite produced in [19] was made by letting short CFRP tapes fall like confetti onto a plate yielding a completely randomised distribution of tape angles in each layer.

2.2.1 Method and Theory - Endcaps

Similar to the tube, the endcaps experiences an evenly distributed pressure, p, over the entire internal surface. In addition to the evenly distributed pressure, the wall thickness t was assumed to be constant, which in combination with the spherical shape resulted in an evenly distributed stress. Under the assumption that the endcaps can be considered thin-walled, the in-plane stresses in spherical coordinates (φ-, θ-directions) are equal and calculated using Equation (18). The out-of-plane stress (r-direction) is approximately equal to zero through the thickness. Equation (18) can also be rearranged and used to calculate the minimum allowed wall thickness t_{min} by using the maximum allowed stress σ_{max}.

$$\sigma_\varphi = \sigma_\theta = \frac{pr}{2t} \tag{18}$$

$$t_{min} = \frac{pr}{2\sigma_{max}} \tag{19}$$

In addition to the internal pressure load, a thermal load with a temperature difference $\Delta T = -383$ °C was applied to the structure as discussed in Section 1.3. This difference in temperature causes a global displacement in the negative r-direction. In addition to the global displacement, the temperature difference cause stresses within the laminate due to the difference in thermal expansion in the longitudinal and transverse directions of the CFRP tapes. In a conventional unidirectional (UD) composite laminate, the stresses due to a change in temperature are trivial to calculate using CLT. Since the material in the endcaps is not made from unidirectional continuous lamina CLT does not readily apply. Nevertheless, CLT can be used to calculate a worst-case scenario in which case the laminate would consist of a [0°/90°] layup. A second option was to use Equivalent Laminate Theory (ELT) where the fibres in each layer are aligned with a predetermined angle but not continuous as in CLT. ELT was presented and used by Mattias Johanssen in [16]. The tapes used in this material are not aligned. Consequently, ELT is not suitable for calculating thermal stresses. For these reasons, CLT was chosen to calculate the worst-case scenario and make sure that the ply stresses in the proposed design were below the limit.

The numerical analysis of the endcaps was done using Abaqus, where the endcap was modelled with homogeneous shell elements and an orthotropic material model including elasticity and thermal expansion. Thus not using a composite layup as for the tube. The rationale for not using a composite layup was that it would require modelling of approximately one million individual CFRP tapes to mimic the material tested in [16]. The use of a homogeneous material in the simulation reduces its validity in the sense that no individual tape stresses nor thermal effects in the interaction of connected tapes can be evaluated.

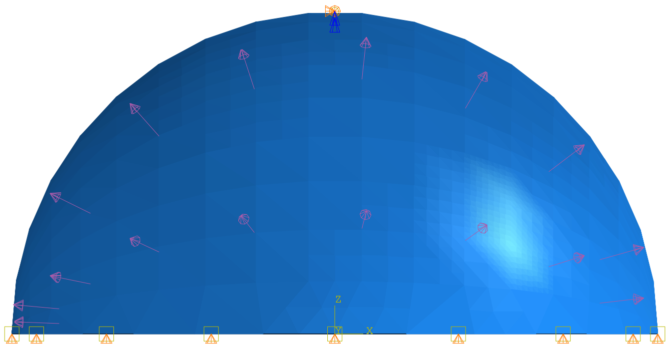

Figure 6: View of Abaqus endcap model with applied boundary conditions and forces. • - surface/edge pressure, • - fixed displacement, • - fixed rotation, • - temperature.

The boundary conditions used in the Abaqus model, shown in Figure 6, were a fixed displacement in the axial direction along the edge connecting the endcap to the tube, still allowing deformation in the radial direction. An internal pressure of 4 bar and a support on a single node on the top of the sphere to prevent rigid body motion. Rigid body motion should not be present in an axisymmetric model like this but due to imperfections in the mesh, rigid body motion occurred when pressure was applied. In addition to the mechanical boundary conditions, a thermal boundary condition was added, similarly as for the tube, a ramped temperature from 130 °C to -253 °C defined as predefined fields.

2.2.2 Results - Endcaps

First of all, the material properties of the uniformly oriented ultra-thin CFRP tape composite were calculated using a MATLAB code provided by [16] where fibre and matrix material properties were taken from Table 1. Some assumptions had to be made of unknown material properties as stated in Section 1.4.1, for example, the fracture toughness G_{IIC} was set to 1200 Jm^{-2}, supported by Nilsson, et al. [20]. The material properties are provided in Table 6 where subscript C denotes composites and represents the in-plane properties of the composite. E_C is Young's modulus of the composite, G_C is the in-plane shear modulus, ν_C is the in-plane Poisson's ratio, α_C is the in-plane thermal expansion, $\hat{\varepsilon}$ is the strain to fail limit and σ_{max} is the corresponding failure stress. The strain to failure and tensile strength depend on the orientation of the failing tape. Persson [16] and Johanssen [19] jointly demonstrated that transverse failure is suppressed for any reasonable value of G_{IIC} where tape pullout takes place as the major failure mode. For very high values of G_{IIC}, even the tape pullout is suppressed and replaced with fibre fracture as the major failure mode.

Table 6: Material properties for uniformly oriented ultra-thin CFRP tape composite.

E_C [GPa]	G_C [GPa]	$\hat{\epsilon}$ [%]	σ_{max} [MPa]	ν_C	α_C [$10^{-6}/°C$]
63	24	1.4	878	0.32	16.2

Once the material properties were set, analytical calculations were made to determine a suitable wall thickness. With the suggested safety factor of 2.5 stated in Section 2.1.2, a wall thickness of 0.85 mm was calculated using Equation (19). This wall thickness is very small compared to the radius, which makes the thin walled assumption in Section 2.2.1 valid. The determined wall thickness resulted in a stress $\sigma_\varphi = \sigma_\theta = 351$ MPa using Equation (18), not considering the safety factor.

The combined thermal and pressure effects on a worst-case scenario layup $[(0/90)_x]$, which creates the largest thermal stresses, was evaluated using CLT and the result is shown in Figure 7 which depicts the through-thickness stresses. Considering that these stresses are for individual plies, the failure stress to compare with are those in Table 2 which shows that all stresses are within their limits and the most critical stress is transverse stress which has a safety factor of 1.2. This safety factor is on the low side and shows that 90° jumps in tape angle are a risk that will occur in a randomised tape angle layup.

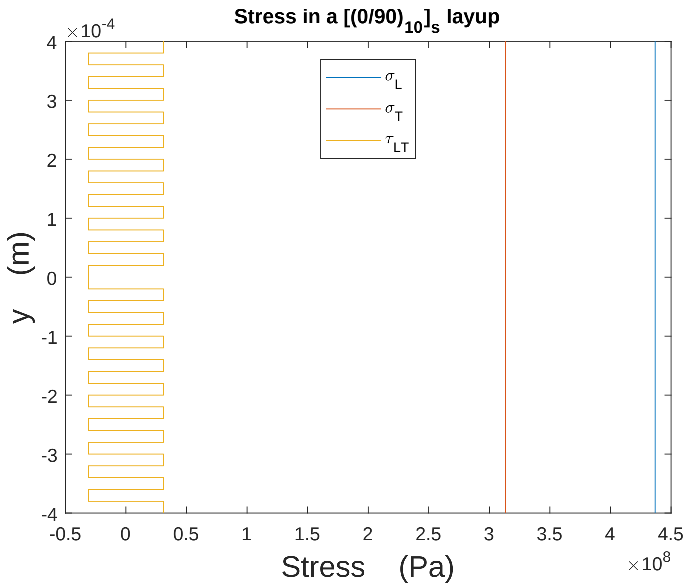

Figure 7: Worst case scenario calculated using CLT including thermal and pressure load.

In addition to analytical calculations, Abaqus was used to perform numerical analysis. To verify that a sufficiently fine mesh was used in the Abaqus simulations, a mesh convergence study was conducted, which result is shown in Figure 8 and shows that 150000 elements with an approximate size of 25 mm^2 are sufficient for this model.

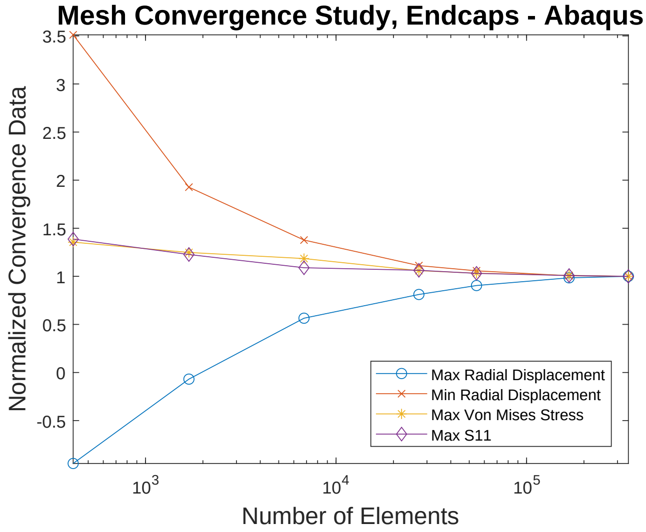

Figure 8: Convergence study with increasing number of elements using normalised units.

To efficiently evaluate stresses, displacements and strains, a spherical coordinate system was implemented. In stress and strain the directional numbering [1, 2, 3] go from representing [x, y, out-of-plane] to represent [θ, φ, out-of-plane]. For the displacement, the numbering represents [r, θ, φ] directions.

The stress in the θ-direction is shown in Figure 9, the maximum stress is 363 MPa whereas the median is approximately 350 MPa which is similar to the analytically calculated stress. The stress should be uniform and corresponding to the analytical solution presented in equation (18) but due to imperfections in the mesh, it is not. The maximum stress in the structure gives a safety factor of $n = \frac{878}{363} = 2.4$, close to the suggested safety factor. In addition, the σ_{22} *i.e.* (S22, φ-direction) stress is, in essence, the same in both magnitude and distribution as the stress shown in figure 9 and the σ_{33} *i.e.* (S33, out-of-plane) stress is zero as expected in this load case.

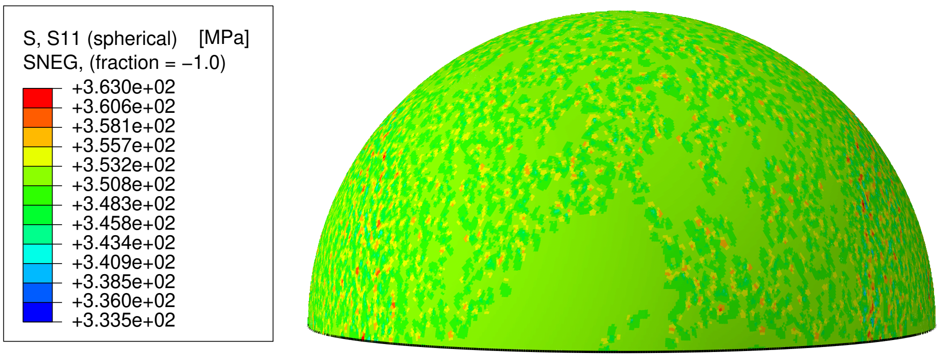

Figure 9: Stress in the theta direction - Abaqus.

The ϵ_{11} *i.e.* (E11, θ-direction) strain is shown in Figure 10 and shows a strain ranging from -0.239% to -0.274%, which is similar for ϵ_{22} *i.e.* (E22, φ-direction) and approximately zero for ϵ_{33} *i.e.* (E33, out-of-plane). A negative strain in combination with positive stress is highly unintuitive and the reasoning behind it is that the reduction in temperature causes a negative strain but no stress. When the pressure is added, positive stress (and strain) is introduced but the added strain is not enough to overcome the negative thermal strain, this is summarised in Table 7. Under the assumption that the magnitude of the fatigue strain limit (ϵ_m=0.6%) is equal in magnitude for negative strains and that maximum tape strain does not exceed the global strain, the endcaps are well within the limit regarding fatigue.

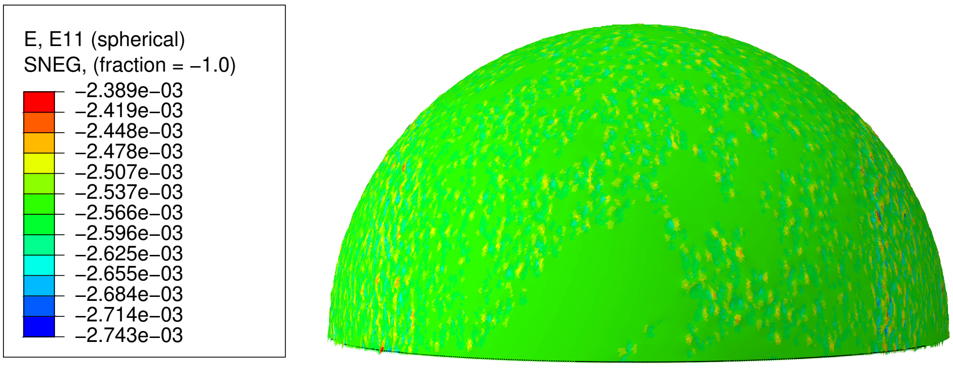

Figure 10: Strain in the theta direction - Abaqus.

Table 7: Thermal, mechanical and total stresses and strains from Abaqus analysis of endcaps with and without thermal/pressure loads.

	ϵ_{11}^{min} [%]	ϵ_{11}^{max} [%]	σ_{11}^{min} [MPa]	σ_{11}^{max} [MPa]
Thermal	-0.6358	-0.6358	0	0
Mechanical	0.3614	0.3969	333.5	363
Total	-0.2744	-0.2389	333.5	363

The final part of the analysis was to evaluate the displacement of the endcap. The relative radial displacement between the endcaps and the tube is critical since a difference in displacement will induce a large strain in the joint. The radial displacement U1 is shown in Figure 11 and ranges from -3.72 mm to -3.9 mm. The negative displacement and strain show that the contraction from the temperature change is larger than the strain induced by the applied pressure, which compares well to the earlier discussion of a negative strain combined with positive stress. The axial direction of the tube experiences the same temperature and stress and reacts in the same way which increases the credibility of the results.

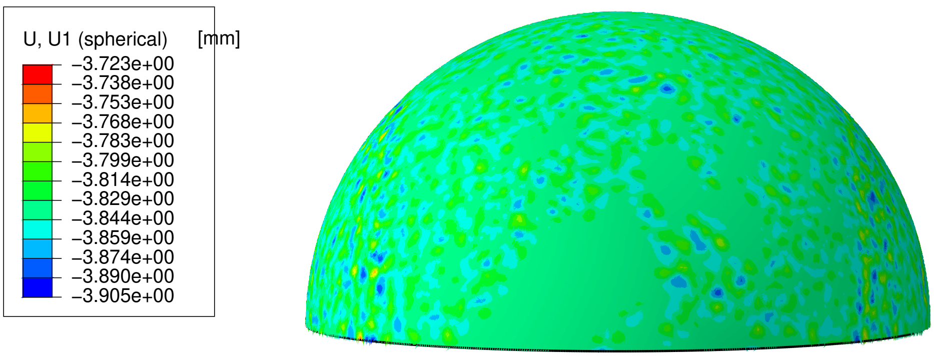

Figure 11: Radial displacement - Abaqus.

2.3 Joint

To join laminates with different thicknesses, two options were discussed: mechanical joints using bolts or rivets and adhesive joints. The mechanical joints require extra sealant materials around the fasteners to prevent leakage and also adds extra weight to the structure. Drilling holes for the fasteners reduces the net cross-sectional area of the structure and introduces localised stress concentrations. These stress concentrations can cause ply delamination since they will include tensile and shear stresses. There is also a risk of corrosion for the mechanical fasteners since the liquid in the tank and moisture in the laminate can be trapped in the crevices inherent in such joints [7].

Adhesive joints do not require extra materials such as sealants other than adhesive chemicals introduced between the two adherents. Since there are no holes in adhesive joints, the risk of localised stress concentrations are eliminated and the load can be distributed over a much wider area than mechanical joints. In addition, the adhesive material is lighter than the metallic fasteners. For these reasons, the adhesive joint was chosen for further investigation.

Different types of adhesive joints, depicted in Figure 12 were reviewed in the project. The single-lap joint was eliminated due to the uneven stress distribution in the adhesive, leaving it vulnerable for peel stress failure. When the singe-lap joint is loaded in-plane, a moment is induced in the joint which creates a rotation and ultimately an uneven stress distribution. It also needs extra sealant implementation to prevent sudden thickness change between laminates of adherent composites. Double lap and double strap joints have some disadvantages regarding assembly of the tank as there are four separate adherents for these types of joints and the inside is difficult to access. The stepped lap, the double stepped lap, and double scarf joints cannot be used in the tank assembly since they need thicker composite structures. In the end, a scarf joint bonded through an adhesive is chosen, this being routinely used within the aerospace industries [7].

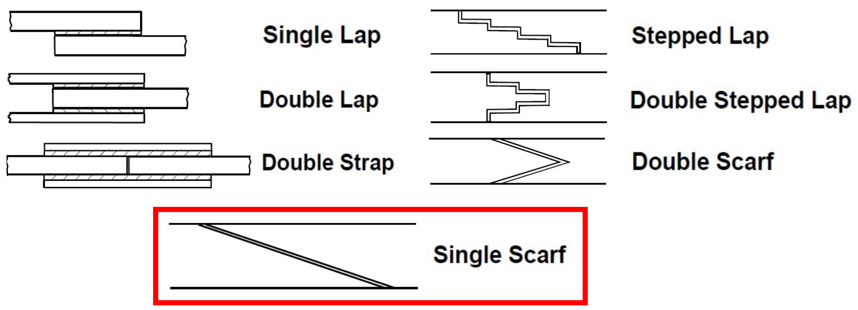

Figure 12: Common adhesive joint configurations.

2.3.1 Method and Theory - Joint

For highly loaded advanced composite structures, length to thickness ratios of the scarf joint ranging from 20:1 to 60:1 are often required for bonded repair patches to restore a damaged structure to its as-designed ultimate strength [21]. The length of the scarf joint have to be based on the endcaps as they have a lower wall thickness than the tube. If the length to thickness ratio is set to 60:1 to maximise the contact surface of the joint and with a wall thickness of 0.85 mm, the length of the joint is 51 mm. In case a 51 mm joint length is too short, a mixture of scarf and single lap joint could be used, as showed in Figure 13 (a). To avoid the discontinuities at the end of the tube in Figure 13 (a), a tapered tube edge can be used. Similarly in Figure 13 (b), the gap can be filled with epoxy to make a smooth transition. Finally, an outer layer of fibres can be added to support the structure as a whole, green layer in Figure 13, but particularly absorb the axial forces induced on the joint. This method is called overwrapping and is further discussed in Section 3.

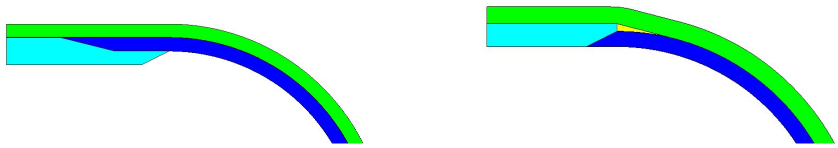

(a) Mixed single lap - scarf joint, tapered tube edge with overwrap.

(b) Scarf joint with epoxy filling and overwrap.

Figure 13: Quarter section cut of the joint area from the front view. Cyan: Tube, Blue: Endcap, Yellow: Epoxy, Green: Overwrapping.

2.3.2 Results - Joint

The displacement results from Sections 2.1.2 and 2.2.2 show that the tube expands in the radial direction whereas the endcaps contract under loading due to the difference in material and stress state. Depending on how the joint is constructed, with either the tube or endcaps on the outside as shown in Figure 13, the joint experiences a compressive or tensile stress during loading. The failure in the adhesive joint is expected to occur first in the adhesive material exposed to peel (tensile) stress, not between the adhesive and adherents as a result of compressive stress. Thus, the outer adherent for the joints was decided to be the endcaps which results in a compressive load on the joints under loading.

The difference between the curing and operational temperature of the tube and endcaps is -383 °C. There will be also a temperature difference due to the refuelling process. These kinds of operational, manufacturing and environmental differences create also different pressure conditions on the tank. Overall, it will be resulted to expose cyclic loads. In the tank assembly, the joints have a higher risk for leakage as a result of external impacts. The fuel leakage from the tank can cause a fatal accident such as an explosion in the aircraft. Adhesively bonded joints have the advantages of these situations that are the good strength for fatigue and the fine sealing properties. Some other advantages and disadvantages of the adhesive joints can be seen in Table 8, [22].

Table 8: General advantages and disadvantages of joints in composites and scarf joints in particular.

Advantages	**Disadvantages**
Excellent fatigue strength.	Significant cure times may be required.
Reduced risk of galvanic corrosion when joining carbon fibres to metals, relevant for external supports.	Jigs and fixtures may be required to locate components whilst the adhesive cures.
No need to have access to the inside of the tank to make the joint.	Rigid process control is required to obtain consistent results.
Bonding is possible on dissimilar materials.	Conventional non-destructive inspection of bonded joints is difficult.
Sealing properties.	Adhesives have poor resistance to peel and cleavage stresses in relation to shear and tension loading.
Weight reduction: Fasteners are not required for the joining.	Adhesives have a finite shelf-life prior to curing and may require special storage conditions before use.

2.4 Full Tank Weight Analysis

In this section, the full tank with the tube connected to the endcaps via the joint will be discussed. The weight of the tank can be calculated by assuming thin walls with the surface area of a cylinder and a sphere.

$$A_{\text{sphere}} = 4\pi r^2, \quad A_{\text{cyl}} = 2\pi r L_c \tag{20}$$

where r and L_c are the radius and the cylinder length of the tank respectively. The total mass of the composite tank can be calculated by

$$M_{\text{composite tank}} = A_{\text{sphere}}\, t_{\text{endcaps}}\, \rho_c + A_{\text{cyl}}\, t_{\text{cyl}}\, \rho_c \tag{21}$$

with ρ_c from Equation (5). This results in a tank mass of $M_{\text{composite tank}} = 110$ kg.

In order to compare these results, calculations were also made for a corresponding steel (STRENX® P700) tank with yield strength $\sigma_{\text{y,steel}} = 700\,\text{MPa}$ and density $\rho_{\text{steel}} = 7800\ \text{kgm}^{-3}$, exposed to the same pressure and with the same dimensions as the composite tank. Metal tanks are commonly designed with a constant thickness based on the maximum stress, the hoop stress. The wall thickness can therefore be calculated using the pressure vessel formulas presented in Equation (17):

$$t_{\text{steel tank}} = \frac{pr}{\sigma_{\text{y,steel}}} \tag{22}$$

The mass of the corresponding steel tank can then be calculated using:

$$A_{\text{tank}} = A_{\text{sphere}} + A_{\text{cyl}} \tag{23}$$

$$M_{\text{steel tank}} = A_{\text{tank}}\, t_{\text{steel tank}}\, \rho_{\text{steel}} \tag{24}$$

The resulting mass of a steel tank was $M_{\text{steel tank}} = 740$ kg. This means the composite tank is roughly 85 % lighter than the steel tank, excluding the added mass of any joints.

Important to keep in mind is that this 85% reduction in mass does not include any added mass from the joint nor any overwrap. In addition, these calculations are based on a stationary tank without consideration of for example landing impact. Thereby a 30 - 50 % reduction as indicated by the NASA project and the CHATT project [11] is more probable for the final product.

3 Proposed Routes for Manufacturing

The manufacturing process of cryogenic pressure vessels may be conducted through a multitude of alternative processes, these having different pros and cons. This section covers the proposal of feasible routes in which the vessel may be produced. Discussing their individual qualities may be used as a guiding source for future research. The methods described may be used individually and combined in alternative ways with newly developed processes if required.

Manufacturing of a pressure tank requires that the structure is hollow, hence it is common within the industry to use a solid core. The core allows for material to be laid on top of it and once removed the result is a hollow product [23]. There are multiple available alternatives that can be used, one option, is to implement a lost core. The principle of this is once the outer material has been either wound or layered on the core, it may be removed without machining of the outer layers. Within the aerospace industry, water-soluble core materials have been used for many years, because they not only provide good results but also attain environmental restrictions. These allow for highly complicated geometries to be created with changes in diameter while simultaneously allowing the core to be washed out. Further improvements are made within this area since it is well used within the aerospace industry. Due to this, it is reasonable to propose this as a feasible manufacturing component. This further allows for the structure to be a one-step production which generally is to be preferred [23]. There may appear issues with this method due to the large geometry of the pressure vessel. The core must be able to carry its own weight, this is not further studied in this report but should be considered when used in this application.

The design of the endcaps is highly dependant on being able to accurately choose both the direction and length of the tapes. This allows for multiple types of fibre placement techniques such as Automated Tape Laying (ATL) and Automated Fibre Placement (AFP). Both allow for the material to be cut and placed precisely however, AFP was developed to overcome the limitations of ATL and also allows for narrower tapes to be placed. Due to this, it is proposed that AFP is used to manufacture the endcaps. Generally, this is used for high-performance structures due to the capability to be placed according to local loading conditions [24]. The process revolves around the computer-controlled laying of tapes with the use of a delivery head as can be seen in Figure 14 . This will be used such that unidirectional tapes can be placed upon the core with full freedom of length and orientation. This also allows for cutouts which commonly is used to make doors and windows on aircraft, in this application it would instead be used to make the holes required for the vessel to function [25].

The tube section of the pressure vessel has different requirements than the endcaps. This led to alternative processes being researched on how to propose a feasible manufacturing method. The layup is more specific in its orientation, implying that a method of creating consistent patterns is required. Currently, within aerospace, it is common to use a form of winding process when creating pressure vessels and tubes. The process uses a rotating mandrel, the tapes would then be set onto the mandrel being continuously under tension (pulling). This method does not allow for discontinuous fibres since cutting would lead to the tapes losing tension and slip out of their designated position on the mandrel however, this function is not sought for the design of the tube. The position implies not only where it is located physically on the mandrel but also the orientation which if lost, negatively affects the structural integrity of the pressure vessel [24]. A visual example of this process being used to manufacture a pressure vessel can be seen in Figure 14.

Within the aerospace industry, it is also common to overwrap pressure vessels, generally, this is typically applied on top of the steel tank as an external support layer [12]. Since the tank proposed within this study is linerless and fully made of composites, the overwrap will instead be added on top of the tube and endcaps. There are numerous advantages to overwrapped pressure vessels, for example, high resistance to fatigue and good strength/stiffness-to-weight ratio [26]. The principle is to reinforce the composite tank with an extra layer of composite material as an overwrap, the structure gains extra support. This is also the case across the joint, allowing the extra material to lower the stress at the connection. Winding angles and patterns are usually chosen based on the strength requirements of the product. It is often a combination of different winding patterns that are used to provide optimal performance [7]. Normally winding is therefore applied in both the longitudinal (helical) and a circumferential (hoop) direction [27]. Further research is required to determine suitable material, winding tension, and the pattern of the wrap. This will not be further detailed in this study, but it is of interest to evaluate the impact of the overwind and if used depends on the requirements of the pressure vessel.

(a) Tape placement on tank designed to hold super cold propellants in a rocket [28]

(b) Filament winding of carbon fiber/epoxy composite pressure vessel [24]

Figure 14: Juxtaposition of tape placement (a) and filament winding (b)

4 Conclusion

In this project, a preliminary design of a lightweight liquid hydrogen tank for future aircraft was proposed and assessed. Thin-ply carbon fibre composites provide a route to liner-less tank solutions at a fraction of the weight of the state-of-the-art metal tanks. As stated in Section 2.4 resulting in a weight reduction of over 85 %, excluding any added weight from the joint nor overwrap.

The different stress and thereby strain states in the hoop of the cylinder and the edge of the spherical endcaps inevitably cause a difference in radial displacement in the two components where the radius of the tube increases but the radius of the endcaps decreases under load in the current design. The difference in displacement will put a high strain on the joint connecting the tube with the endcaps. The obvious way of achieving an equal displacement of the two parts without reducing the safety factor is to increase the wall thickness of the tube, reducing the mechanical stresses in the hoop. Another solution is to reduce the initial radius of the cylinder so that when the in-use thermal and pressure loads are applied and the cylinder and sphere radii expands and contracts respectively, the two meet in the middle. As a result, the joint is in a stress free state at the in-use application. This also means that the joint is in a stressed state when no pressure and temperature are applied which could be a risk and would have to be outlined in the operating guidelines of the tank.

If the tank is designed so that the tube is initially smaller radially than the endcaps, the discussion about having the endcaps on the outside in Section 2.3.2 is no longer valid. If the endcaps are on the outside and the stress free state of the joint is during loading, the joint will experience a very high peel stress when it is not loaded. Instead, the tube should be on the outer part of the joint so that a compressive force is placed upon the joint in the relaxed, unloaded state.

Theoretical studies of the proposed design indicate its feasibility. However, this has to be verified in practice by the manufacture and experimental demonstration.

5 Future Work

As this project concerns a preliminary design, the list of future work is long and only the major parts of necessary future work will be brought up in the following paragraphs. Important to note is that this is not a project that should nor could be rushed to production without first doing the necessary computations and testing as mistakes could lead to catastrophic failure and loss of life.

The initial step towards a final design is to validate the material data used in the calculations. This should be done through material testing, initially of test specimens, and during the evolution of the project more application-like parts. One area of interest is to test the permeation properties of a thin-ply laminate to confirm that a liner is indeed not necessary. Another area of interest is to test the material in real use temperature as most previous temperature-dependent material testing has been done using liquid nitrogen that has a boiling temperature of -195.79 °C at sea level.

Another aspect of future work is to perform in-use simulations that take external factors such as landing, take-off, and external turbulence into account. These simulations should use a mix of fluid and solid mechanics so that phenomena like sloshing can be identified and prevented. In addition, a suitable thermal insulator must be investigated to reduce the cooling requirement of the tank.

A mechanical aspect that has only been assessed qualitatively in this preliminary design is fatigue. The impact of fatigue in the tank should be investigated further both with simulations and testing to prove that the tank can stand multiple use cycles.

The manufacturing processes established in Section 3 are primarily included as a direction in which further research can be conducted. The implementation of these in the construction of the liquid hydrogen tank requires additional experimental data. The usage of overwinding and AFP is well established in the industry to this specific application. In terms of the uniformly oriented ultra-thin discontinuous CFRP tape composite material, it is yet to be studied as a material source for this application. It would therefore be of great interest to conduct further research in this area, more specifically on how well these newly developed thin-ply materials handle the conditions of the pressure vessel.

As a final note, it should be addressed that this project was conducted by five engineering students and the main aspect of the project has been mechanical evaluation. Some non-engineering aspects that should be investigated further are the economic, ethical, and environmental impact, not only of this project but also of the phasing out of fossil fuels in benefit of hydrogen. One interesting topic here is how the production of clean hydrogen is more likely to benefit developed countries with an established source of clean energy whereas developing countries might not have the same access to clean energy to produce clean hydrogen.

References

[1] European Union, "A hydrogen strategy for a climate-neutral europe," Jul. 2020. [Online]. Available: https://eur-lex.europa.eu/legal-content/EN/TXT/?uri=CELEX:52020DC0301.

[2] Airbus. (2020). "Airbus reveals new zero-emission concept aircraft," [Online]. Available: www.airbus.com/newsroom/press-releases/en/2020/09/airbus-reveals-new-zeroemission-concept-aircraft.html. [Accessed: 2021-04-09].

[3] H. Nojoumi, I. Dincer, and G. Naterer, "Greenhouse gas emissions assessment of hydrogen and kerosene-fueled aircraft propulsion," *International Journal of Hydrogen Energy*, vol. 34, no. 3, pp. 1363–1369, 2009. DOI: https://doi.org/10.1016/j.ijhydene.2008.11.017.

[4] Office of Energy Efficiency & Renewable Energy. (n.d.). "Hydrogen Storage," [Online]. Available: https://www.energy.gov/eere/fuelcells/hydrogen-storage. [Accessed: 2021-04-19].

[5] Shell. (2020). "Civil jet fuel," [Online]. Available: https://www.shell.com/business-customers/aviation/aviation-fuel/civil-jet-fuel-grades.html. [Accessed: 2021-04-09].

[6] D. Matsson, A. Kopp, K. Olofsson, G. Kurth, E. Roorda and E. Mooij, "The aurora space launcher concept," in *Deutsche Luft- und Raumfahrtkongress (DLRK) 2016*, Sep. 2016. [Online]. Available: https://elib.dlr.de/107566/.

[7] B. D. Agarwal, L. J. Broutman, and K. Chandrashekhara, *Analysis and Performance of Fiber Composites*. Hoboken, New Jersey: John Wiley and Sons, 2018, p. 258, ISBN: 9781119390008.

[8] B. A. Sandoval Rosales, "Thin-ply CFRP for cyogenic fuel tank applications," M.S. thesis, Luleå University of Technology, Luleå, Sweden, 2019.

[9] M. Alves, D. Carlstedt, F. Ohlsson, L. Asp, and S. Pimenta, "Ultra-strong and stiff randomly-oriented discontinuous composites: Closing the gap to quasi-isotropic continuous-fibre laminates," *Composites Part A: Applied Science and Manufacturing*, vol. 132, p. 105 826, 2020, ISSN: 1359-835X. DOI: 10.1016/j.compositesa.2020.105826.

[10] G. Chauhan and A. Awasthi, "Design and analysis of high pressure composite vessels," vol. Volume -03, Jul. 2018.

[11] M. Sippel, A. Kopp, D. Mattsson, and S. Koussios, "Advanced Cryo-Tanks Structural Design Investigated in CHATT," Mar. 2014. [Online]. Available: https://elib.dlr.de/89206/.

[12] S. Alam, G. R. Yandek, R. C. Lee, and J. M. Mabry, "Design and development of a filament wound composite overwrapped pressure vessel," *Composites Part C: Open Access*, vol. 2, p. 100 045, 2020, ISSN: 2666-6820. DOI: 10.1016/j.jcomc.2020.100045.

[13] Boeing Commercial Airplanes. (Jul. 2019). "737 max, airplane characteristics for airport planning," [Online]. Available: https://www.boeing.com/resources/boeingdotcom/commercial/airports/acaps/737MAX_RevE.pdf. [Accessed: 2021-05-16].

[14] PVEng. (2019). "Comparison between head types: Hemi, se, fd and flat," [Online]. Available: https://www.pveng.com/home/asme-code-design/comparison-between-head-types-hemi-se-fd-and-flat/. [Accessed: 2021-05-05].

[15] R. Talreja, "Damage and fatigue in composites - a personal account," *Composites Science and Technology - COMPOSITES SCI TECHNOL*, vol. 68, pp. 2585–2591, Oct. 2008. DOI: 10.1016/j.compscitech.2008.04.042.

[16] M. Persson, "Mechanical analysis methods for ultra-stiff CFRP from thin tapes," M.S. thesis, Chalmers University of Technology, Gothenburg, Sweden, 2019.

[17] R. Auenhammer, *Help with fe-analysis and abaqus related issues*, personal communication, Apr. 13, 2021.

[18] P. Linde, *Lecture on the aircraft industry in general and, liquid hydrogen fueled aircraft in particular*, personal communication, Apr. 15, 2021.

[19] M. Johanssen, "Manufacturing and characterisation of ultra-stiff composite material," M.S. thesis, Chalmers University of Technology, Gothenburg, Sweden, 2019.

[20] K.-F. Nilsson, L. Asp, J. Alpman, and L. Nystedt, "Delamination buckling and growth for delaminations at different depths in a slender composite panel," *International Journal of Solids and Structures - INT J SOLIDS STRUCT*, vol. 38, pp. 3039–3071, Apr. 2001. DOI: 10.1016/S0020-7683(00)00189-X.

[21] C. H. Wang and A. Gunnion, "Design methodology for scarf repairs to composite structures," vol. 44, p. 6, Aug. 2006.

[22] C. Worrall, E. Kellar, and C. Vacogne. (Jan. 2020). "Joining of fibre-reinforced polymer composites," [Online]. Available: https://compositesuk.co.uk/system/files/documents/Joining%20Good%20Practice%20Guide%20-%20FINAL.pdf. [Accessed: 2021-05-17].

[23] J. Kaerger and L. Atz, "Water soluble mandrels for lost core applications in manufacturing of hollow composite structures," Oct. 2019, pp. 1–2.

[24] S. Beckwith, "Filament winding vs. fiber placement manufacturing technologies," vol. 44, pp. 54–55, Mar. 2008.

[25] A. Crosky, C. Grant, D. Kelly, X. Legrand, and G. Pearce, "4 - fibre placement processes for composites manufacture," in *Advances in Composites Manufacturing and Process Design*, P. Boisse, Ed., Woodhead Publishing, 2015, pp. 79–92, ISBN: 978-1-78242-307-2. DOI: 10.1016/B978-1-78242-307-2.00004-X.

[26] Q. Wu, X. Chen, Z. Fan, and D. Nie, "Stress and damage analyses of composite overwrapped pressure vessel," *Procedia Engineering*, vol. 130, pp. 32–40, 2015, Pressure Vessel Technology: Preparing for the Future, ISSN: 1877-7058. DOI: 10.1016/j.proeng.2015.12.171.

[27] P. B. McLaughlan, S. C. Forth, and L. R. Grimes-Ledema, "Composite overwrapped pressure vessels, a primer," Mar. 2011. [Online]. Available: https://ntrs.nasa.gov/api/citations/20110008406/downloads/20110008406.pdf.

[28] McMahan, Tracy and Anderson, Janet. (Aug. 2017). "Move over heavy metal, there's a new tank coming to town," [Online]. Available: https://www.nasa.gov/centers/marshall/news/news/releases/2014/14-043.html. [Accessed: 2021-05-21].